

A perturbation theory and simulations of the dipole solvation thermodynamics: Dipolar hard spheres

Dmitry V. Matyushov^{a)} and Branka M. Ladanyi
Department of Chemistry, Colorado State University, Fort Collins, Colorado 80523

(Received 15 June 1998; accepted 2 October 1998)

Padé truncation of the thermodynamic perturbation theory is used to calculate the solvation chemical potential of a dipolar solute in a model fluid of dipolar hard spheres. Monte Carlo simulations of the solvation thermodynamics are carried out over a wide range of solute and solvent dipoles in order to address the following major issues: (i) testing the performance of the Padé perturbation theory against simulations, (ii) understanding the mechanism of nonlinear solvation, and (iii) elucidating the fundamental limitations of the dielectric continuum picture of dipole solvation. The Padé form of the solvation chemical potential constructed in the paper agrees with the whole body of simulation results within an accuracy of 3%. Internal energy and entropy of solvation are also accurately described by the perturbation treatment. Simulations show a complex nonlinear solvation mechanism in dipolar liquids: At low solvent polarities the solvation nonlinearity is due to orientational saturation that switches to the electrostriction mechanism at higher dipolar strengths of the solvent. We find that the optimum cavity radius of the Onsager reaction-field theory of solvation depends substantially on solvent polarity. A general method of testing the performance of linear solvation theories is proposed. It shows that the fundamental failure of continuum theories consists in their inaccurate description of the internal energy and entropy of solvation. © 1999 American Institute of Physics. [S0021-9606(99)04301-9]

I. INTRODUCTION

Understanding of the static and dynamic properties of optical transitions of a chromophore immersed in a liquid solvent demands accurate description of dipole solvation.¹ With the aim of future application to optical spectroscopy, our present study was motivated by three main tasks: (i) testing the performance of perturbation theories of dipole solvation against computer simulations, (ii) understanding the nonlinear solvation mechanism, and (iii) revealing fundamental limitations of dielectric continuum models of solvation for the simple model system of a dipolar solute in a dipolar solvent.

Perturbation theories have been used since the earliest days of statistical mechanics,^{2(a)} but in liquid state applications they eventually have given way to more accurate integral equation theories^{2(b)} and computer simulations.^{2(c)} The main disadvantage of using perturbation expansions in liquid state calculations is the absence of a small parameter rendering expansions slowly converging. Stell and co-workers suggested a way of overcoming this difficulty in a phenomenological way by truncating the perturbation series in the long-ranged part of the potential in a form of a Padé approximant usually including two-particle and three-particle intermolecular correlations and neglecting all higher-order terms.^{2(b),3} This approximation proved to be outstandingly successful for different types of intermolecular potentials.^{2(b)} Its main success was in treating thermodynamics of long-range multipolar forces for which the convergence of pertur-

bation expansions is especially poor. Among the merits of the Padé solution for thermodynamic properties of polar liquids is its analytical simplicity and ease of including the molecular (generally anisotropic) polarizability.⁴

Recently, we have exploited the advantages of the Padé truncation approach for calculating the solvation chemical potential μ_p of a dipole in dipolar (nonpolarizable and polarizable) liquids.⁵ The method was also used to include nonlinear solvation.^{5(b)} This was achieved by Padé truncating the perturbation expansion in the dipolar part of the solute-solvent interaction potential resulting in the dependence on the solute dipole moment m_0 in the form

$$\beta\mu_p = -\frac{am_0^2}{1+bm_0^2}. \quad (1)$$

This equation predicts saturation of the dipolar response at high magnitudes of the solute dipole moment and the function $\mu_p(m_0)$ has simple poles in the complex plane of m_0 at $m_0 = \pm i/\sqrt{b}$. The range between the two singularities $-i/\sqrt{b} \leq m_0 \leq i/\sqrt{b}$ determines the width of a band of permissible fluctuations of the solute energy that can be produced by a dipolar fluid.^{5(c)} The existence of a confined fluctuation band perhaps cannot be proved directly, but it manifests itself, indirectly, in optical spectroscopy.^{5(c)} Application of Eq. (1) to the calculation of optical bandshapes results in nonlinear compression of optical bands and several other effects that can be extracted from experimental spectroscopic data. In view of the potential importance of these predictions, we pursue here two goals: testing the numerical accuracy of the chemical potential (1) and confirming the nonlinear dependence on the solute dipole given by the Padé

^{a)}Present address: Department of Chemistry, University of Utah, Salt Lake City, UT 84112.

form (1). To achieve these goals we need to test separately the linear, a , and nonlinear, b , response coefficients in Eq. (1). We do that in Sec. III B by measuring moments of the solute-solvent interaction potential and a mixed second moment of the solute-solvent and solvent-solvent potentials on the system configurations created by Monte Carlo (MC) simulations.^{2(c)} We find that the b coefficient obtained from perturbation expansion conforms well with simulations, whereas the linear response coefficient a needs correction at high solvent polarities. With the correction of a proposed in Sec. III B we achieve an agreement within 3% with the simulation results.

Simple molecular models have a tremendous potential for providing valuable insights into fundamentals of solvation in liquids. This is because, by choosing a suitable model, one can study a particular feature of the complex process of equilibrium solvation in molecular liquids. This strategy was recently followed by Papazyan and Warshel,⁶ who analyzed the cavity concept of dielectric continuum theories of solvation for a model system of ionic and dipolar solutes in a dipolar lattice. In that way, they examined the effect of the purely orientational response. The fitted cavity radii turned out to be different for a charge and a dipole and showed a significant variation as a function of solvent polarity.

The main components of polar solvation⁷ in real liquids are: (1) orientational response and (2) density response. The latter is a complex phenomenon including: (i) fluctuations of the local solvent density, (ii) changes in the average solvent-solvent separations, and (iii) variations of the equilibrium distances between solute and solvent molecular groups with changing attractive potential.^{8,9} The first component, (i), enhances, on average, the solvation stabilization energy in the linear response. The combination of (ii) and (iii) is called electrostriction in the literature.¹⁰ This is a nonlinear solvation effect. One may argue that it is electrostriction [(ii) and (iii)] that compensate for the failure of continuum models to describe the orientational response.⁶ Our present paper makes a next step, compared to the dipolar lattice model explored by Papazyan and Warshel,⁶ toward realistic liquid solvation. We explore here solvation of a hard sphere (HS) dipolar solute in a dipolar fluid. In this case, both orientational rearrangement [orientational response, (1)] and local density changes in the solvent are allowed. On the other hand, because of the hard repulsive potential, the equilibrium solute-solvent distance and hence the position of the first peak of the solute-solvent pair distribution function is fixed by the choice of the solute and solvent sizes and does not change with the solute and solvent dipole moments. There is, therefore, no complication of compressing the solute and solvent molecular cores in the solvation process that, in our model, includes the components (1), (i), and (ii).

The basic concept of linear response theories is to express solvation through a response function that depends on homogeneous solvent properties. HS dipolar fluids are fully characterized by two parameters: the reduced solvent density $\rho^* = \rho\sigma^3$ and the reduced dipole moment $m^{*2} = \beta m^2/\sigma^3$. Here ρ and σ are, respectively, the number density and the HS solvent diameter, m is the solvent permanent dipole, and $\beta = 1/k_B T$. In a molecular description of solvation, the solute

chemical potential can be determined in terms of ρ^* and m^* and, additionally, the solvent diameter σ , the solute radius R_0 , and the solute dipole moment m_0 . In the dielectric continuum ansatz, one needs only one bulk solvent parameter, the static dielectric constant ϵ , and, for the solute, the cavity radius R_{cav} that is not specified, but is assumed to be independent of the solvent. Hence, we have two parameter sets $\{m^*, \rho^*, \sigma, m_0, R_0\}$ and $\{\epsilon, R_{\text{cav}}, m_0\}$ for molecular and continuum treatments, respectively. The advantage of continuum models is clearly a smaller number of parameters and simpler expressions for the solvation free energy. The disadvantage is the unknown cavity radius and several attempts at its construction have been made in the literature.^{8(b),8(c),9,11} The basic question that remains open is whether a cavity radius determined in the framework of some procedure is independent of the solvent. A noticeable and complicated dependence on solvent polarity and density would depreciate all the advantages of the dielectric continuum approach.

We analyze the optimum cavity size in Sec. III B below. To do that we need bulk dielectric constants of dipolar fluids of various polarities. We obtain these from MC simulations of pure solvent in Sec. II. We turn to solvation thermodynamics in Secs. III and IV. As in the case of dipolar lattices, we find in Sec. III that the fitted cavity radius varies substantially with solvent polarity. In Sec. IV, we propose a general approach to testing linear solvation theories that is independent of the method used to define the solute (cavity) size provided the latter does not change with the solvent dipole moment. We find that the dependence of the cavity radius on solvent polarity leads to a wrong splitting of the solvation free energy into the internal energy and entropy components in continuum treatments assuming $R_{\text{cav}} = \text{const}$. Finally, Sec. V concludes with the discussion of qualitative features of dipole solvation.

II. DIELECTRIC CONSTANT

The problem of calculating static dielectric constants of dipolar fluids is important in its own right and numerous simulations of HS dipolar,¹² Stockmayer,¹³ and soft dipolar¹⁴ fluids have been reported in the literature. Early simulations of dipolar fluids suffered from inadequate sampling, incorrect implementation of the boundary conditions theory, and lacked error estimates (for a review, see Refs. 15 and 16). With the recent shift of interest to more realistic liquid models,¹⁷ calculation of the dielectric parameters of simple model liquids was mostly abandoned. As a result, for dipolar HS fluids, only a few dielectric constants are known with acceptable accuracy.

Early comparison of simulation results for model dipolar fluids to the linearized hypernetted-chain (LHNC)¹⁸ theory proved to be unfavorable for highly polar liquids.¹⁶ No conclusion could thus be drawn concerning the accuracy of approximate theories and the adequacy of simulation techniques. The more recent nonlinear reference hypernetted-chain (RHNC) theory developed by Fries and Patey¹⁹ showed, however, a reasonable agreement between simulated and calculated dielectric constants for $(m^*)^2 \leq 2$ and $\rho^* = 0.8$. Also the perturbation theory (PT) of Tani *et al.*^{20(a)}

gives dielectric constants very similar to both simulations and RHNC.^{20(b)} Based on these findings one may be more confident about general applicability of the schemes developed to extract infinite-size dielectric parameters from finite-volume simulations of dipolar liquids.^{2(c),15,16} Below we report the results of our MC simulations of HS dipolar fluids in the polarity range $1.0 \leq m^* \leq 3.75$ which we compare to RHNC and PT treatments.

A common way to obtain the static dielectric constant is through the Kirkwood factor

$$g_K = \frac{\langle \mathbf{M}^2 \rangle}{Nm^2}, \quad (2)$$

where

$$\mathbf{M} = \sum_{j=1}^N \mathbf{m}_j \quad (3)$$

is the total dipole moment of a dipolar liquid composed of a macroscopic number of N molecules. g_K is related to ε by the standard equation

$$\frac{(\varepsilon - 1)(2\varepsilon + 1)}{9\varepsilon} = yg_K, \quad (4)$$

where $y = (4\pi/9)\beta m^2 \rho$ is the density of the liquid dipoles. In the present paper, we will calculate dielectric constants from the constant volume MC simulations carried out on the cubic simulation cell with the spherical reaction field (RF) boundary conditions^{2(c),15,16} applied to treat long-ranged dipole-dipole forces. It is now well documented that boundary conditions employed in a computer simulation of polar fluids have a large impact on the simulated finite-volume Kirkwood factor

$$G_K(\varepsilon') = (Nm^2)^{-1} [\langle \mathbf{M}^2 \rangle_V - \langle \mathbf{M} \rangle_V^2], \quad (5)$$

where $\langle \dots \rangle_V$ indicates the average over the finite simulation volume V . G_K depends on the value of the reaction field dielectric constant ε' used to determine the RF cutoff of the interaction potential. Two fluctuation formulas connecting $G_K(\varepsilon')$ with the bulk dielectric constant ε have been proposed. The first relation is by Neumann^{13(b),21} that states

$$\frac{(\varepsilon - 1)(2\varepsilon' + 1)}{(2\varepsilon' + \varepsilon)} = 3yG_K(\varepsilon'). \quad (6)$$

A somewhat different fluctuation formula was proposed by de Leeuw *et al.*,¹⁵

$$\frac{(\varepsilon - 1)(2\varepsilon' + 1)}{(2\varepsilon' + \varepsilon)} = 3\gamma y G_K(R_c, \varepsilon'), \quad (7)$$

where

$$G_K(R_c, \varepsilon') = (Nm^2)^{-1} [\langle \mathbf{M}(R_c) \cdot \mathbf{M} \rangle_V - \langle \mathbf{M}(R_c) \rangle_V \cdot \langle \mathbf{M} \rangle_V], \quad (8)$$

$$\mathbf{M}(R_c) = (N)^{-1} \sum_{k=1}^N \sum_{j=1}^N \mathbf{m}_k \theta(R_c - r_{jk}), \quad (9)$$

$\theta(x)$ is a step function and R_c is the RF cutoff distance. For the spherical RF cutoff with $R_c = L/2$ (L is the side length of

the cubic simulation box) that we use throughout below, γ in Eq. (7) is equal to $6/\pi$. Early simulations of dipolar fluids also employed the definition of the Kirkwood factor through the angular $h^{110}(r)$ projection of the pair correlation function¹⁶

$$G'_K(R_c, \varepsilon') = 1 + (4\pi\rho/3) \int_0^{R_c} r^2 h^{110}(r) dr. \quad (10)$$

In his molecular dynamics (MD) simulations of a fluid of soft dipolar spheres, Kusalik reported a substantial variation of the dielectric constant with both the number of molecules in the simulation box and the RF dielectric constant ε' used in defining the boundary conditions.¹⁴ We therefore set up calculations with the aim of examining the system size and ε' dependence of the dielectric parameters. The MC simulations of dipolar HS fluids were carried out using Metropolis sampling with RF boundary conditions for the canonical NVT ensemble^{2(c)} in a cubic simulation box with the side length L , the cut-off distance $R_c = L/2$, and the acceptance ratio for MC moves equal to 0.5. Table I summarizes the infinite-size dielectric constants and Kirkwood factors obtained from Eqs. (4) to (9) for dipolar fluids at $\rho^* = 0.8$ and $(m^*)^2 = 3.0$ with varying numbers of particles, $N = 256, 500,$ and 864 , and two values of the RF dielectric constant. The system total dipole moments \mathbf{M} [Eq. (3)] and \mathbf{M}_c [Eq. (9)] and their first and second moments were calculated after the equilibration period of 50 000 cycles.

The RF method, by construction, implies that ε' must be close to the dielectric constant ε of the bulk liquid. However, the optimum value of ε' may differ from ε and the choice is dictated by a compromise between the errors of evaluating G_K increasing with decreasing ε' and the necessity to maximize sampling of the phase space.¹⁵ For soft dipolar fluids, Kusalik claimed^{14(a)} that $\varepsilon' \approx \varepsilon$ is the best choice when used in MD simulations with periodic boundary conditions. In view of this, we also performed simulations with ε' adjusted during simulation runs using the iterative self-consistent method recently proposed by Gil-Villegas *et al.*²² in application to phase stability of dipolar spherocylinders. In this procedure the Kirkwood factor $G_K(\varepsilon')$ [Eq. (5)] was calculated for the first 10^4 cycles with $\varepsilon' = 100$ and then was used to determine the dielectric constant ε from Eq. (6). This latter value was then used as the RF dielectric constant and was updated every 10^3 cycles. The results of this procedure are also listed in Table I for $N = 256$ and 500 .

We can draw several conclusions from examining Table I. First, there is no regular dependence of ε on the system size for $\varepsilon' = 1000$. As is illustrated in Fig. 1, the convergence of simulations slows down with increasing N . For $N = 256$, G_K factors reach stationary values after $N_c \approx 230$ 000 cycles and we obtain a relatively long plateau on which G_K listed in Table I is measured. For $N = 500$ and 864 particles the stationary values are reached only at the end of simulation runs and no good statistics were achieved. Second, for $\varepsilon' = 10$ the convergence is much faster, but the errors are higher. The iterative self-consistent procedure of determining ε' in the course of simulation runs proves to converge very slowly and we could not achieve long enough plateaus. There-

TABLE I. Dielectric constants and Kirkwood factors at different numbers of solvent molecules and RF dielectric constants ϵ' for dipolar HS fluids at $\rho^*=0.8$ and $(m^*)^2=3.0$. N_c^{\max} denotes the number of simulation cycles.

ϵ'	$N_c^{\max}/1000$	ϵ				g_K		
		Eq. (6)	Eq. (6) ^a	Eq. (7)	Eq. (7) ^b	Eq. (6)	Eq. (7)	Eq. (10)
256 particles								
10	400	94±5	97±6	97±7	100±7	6.2±0.4	6.4±0.4	<0
78 ^c	400	77	83	77	84	5.06	5.09	6.04
1000	350	92.3±0.6	96.4±0.7	91.9±0.5	96.0±0.7	6.09±0.04	6.06±0.06	8.38
500 particles								
10	350	73±2	74±2	74±2	75±1	4.8±0.18	4.9±0.1	<0
89 ^c	400	89	94	89	94	5.84	5.86	6.08
1000	450	86.1±0.3	88.7±0.2	85.9±0.3	88.3±0.2	5.68±0.02	5.66±0.02	8.34
864 particles								
1000	300	94.8±0.8	96.7±0.5	94.6±0.8	96.7±0.5	6.25±0.05	6.24±0.05	9.11

^aWith $\langle \mathbf{M}^2 \rangle_V$ instead of $\langle \delta \mathbf{M}^2 \rangle_V$ in Eq. (5).

^bWith $\langle \mathbf{M} \cdot \mathbf{M}_c \rangle_V$ instead of $\langle \mathbf{M} \cdot \mathbf{M}_c \rangle_V - \langle \mathbf{M} \rangle_V \langle \mathbf{M}_c \rangle_V$ in Eq. (8).

^cWith the self-consistent dielectric constant of the RF as described in the text. Because of poor convergence the values listed are averages at the end of simulation runs.

fore, only dielectric parameters at the end of simulation runs are listed in Table I.

The rate of simulation convergence can be judged from the comparison of dielectric parameters obtained from the second moments $\langle (\delta \mathbf{M})^2 \rangle_V$ and $\langle \delta \mathbf{M}_c \cdot \delta \mathbf{M} \rangle_V$ to the same quantities obtained from the expectation values $\langle \mathbf{M}^2 \rangle_V$ and $\langle \mathbf{M}_c \cdot \mathbf{M} \rangle_V$ in Eqs. (5) and (8). The two ways must be identical for a macroscopic isotropic liquid and the small ratio $\langle \mathbf{M} \rangle_V^2 / \langle \mathbf{M}^2 \rangle_V$ serves as an indication of the adequate sampling of the phase space.¹⁵ This ratio decreases with increasing N_c but remains nonzero at $(m^*)^2=3.0$, resulting in slightly different dielectric constants (Table I). Note in this respect that the use of second moments is more accurate for

finite-volume simulations.¹⁵ The difference between the two ways of determining G_K factors can be seen only for highest polarities $(m^*)^2 \geq 3.0$ and already for $(m^*)^2=2.5$ we eventually do not see any difference between $\langle \mathbf{M}^2 \rangle_V$ and $\langle (\delta \mathbf{M})^2 \rangle_V$ for $N_c > 100\,000$.

For a comparison to finite-volume Kirkwood factors $G_K(\epsilon')$ and $G_K(R_c, \epsilon')$ we also showed in Fig. 1 the contact value $h_{ss}^{110}(\sigma^+)$ of the $h_{ss}^{110}(r)$ angular projection of the liquid pair distribution function (the subscript “ss” stands for solvent-solvent). As is seen, it converges much faster than the Kirkwood factors $G_K(\epsilon')$ and $G_K(R_c, \epsilon')$. However, as shown in Table I, the use of Eq. (10) does not give qualitatively correct values for high ϵ' and results in unphysical negative g_K at $\epsilon'=10$. There is also a considerable dependence on the system size. The reason is a high sensitivity of G'_K to the cutoff distance, since a considerable portion of the integral in Eq. (10) comes from the long-range part of $h_{ss}^{110}(r)$.¹⁶

Table I also shows that the two methods of determining the infinite-volume dielectric constant from Eqs. (6) and (7) are equivalent not only for the average ϵ , but also for its standard deviation. Therefore, the calculations are not in fact sensitive to the molecules at the corners of the simulation cell that are excluded in the method of de Leeuw *et al.*¹⁵ The same conclusion was reached by Kusalik *et al.*^{14(c)} in application to soft dipolar spheres.

The main result of the analysis performed here is that, as long as we have at least 256 particles in the simulation box, it is not the system size that is most important in simulating dipolar HS fluids when $\epsilon' > \epsilon$. The main concern in obtaining a reliable value of the dielectric constant is adequate sampling of the phase space achieved by sufficiently long simulation runs. We therefore tabulated dielectric constants at different solvent polarities by simulating the system of $N=256$ molecules with $\epsilon'=1000$. The number of simulation cycles was chosen to assure a stationary value of the finite-size Kirkwood factor G_K for at least 100 000 cycles. The values of G_K used to calculate ϵ and g_K and their standard

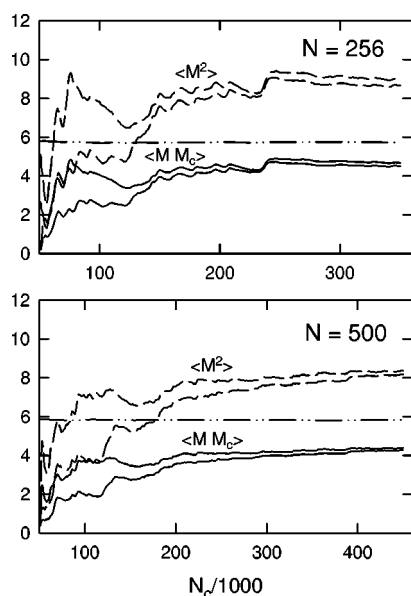


FIG. 1. Dependence of the finite-size Kirkwood factors calculated from Eq. (5) (dashed lines) and Eq. (8) (solid lines). $\langle M^2 \rangle$ and $\langle M M_c \rangle$ indicate the Kirkwood factors with the expectation values $\langle \mathbf{M}^2 \rangle_V$ and $\langle \mathbf{M} \cdot \mathbf{M}_c \rangle_V$ used instead of the corresponding second moments in Eqs. (5) and (8). The dash-dotted lines show contact values $h_{ss}^{110}(\sigma^+)$.

TABLE II. Dielectric parameters and internal energies per molecule $\langle U_{ss} \rangle_V / N$ of dipolar fluids of different polarity at $\rho^* = 0.8$. Simulations are carried out at $\epsilon' = 1000$ and $N = 256$. N_c^{\max} denotes the number of simulation cycles.

$(m^*)^2$	$N_c^{\max}/1000$	$-\beta \langle U_{ss} \rangle_V / N$			ϵ				$\frac{g_K}{MC}$
		MC	Ref. 19 ^a	RHNC	MC	Ref. 19	PT	RHNC	
1.00 ^b	250	1.001 ± 0.001	1.00	0.97	7.96 ± 0.03	9.0 ± 0.5	9.15	8.78	1.48 ± 0.06
1.50 ^b	250	1.833 ± 0.002		1.76	16.8 ± 0.1		18.0	17.4	2.15 ± 0.01
2.00	250	2.753 ± 0.002	2.66	2.63	30.0 ± 0.2	31.6 ± 4	31.1	31.2	2.94 ± 0.02
2.50 ^b	250	3.715 ± 0.002		3.56	51.7 ± 0.2		49.3	57.6	4.07 ± 0.02
2.75	250	4.235 ± 0.002	4.21	4.05	67.5 ± 0.7	65 ± 3	60.5	82.5	4.85 ± 0.05
3.00	350	4.744 ± 0.006			92.3 ± 0.5		73.2		5.22 ± 0.12
3.25	350	5.279 ± 0.007			128.5 ± 1.5		87.6		7.83 ± 0.09
3.50	400	5.815 ± 0.007			149 ± 2		103.8		8.42 ± 0.15
3.75	400	6.357 ± 0.007			218 ± 3		121.8		11.5 ± 0.17

^aResults of previous simulations of dipolar liquid listed in Ref. 19.

^bWith $N = 500$.

deviations were obtained by averaging over these last 100 000 cycles. The simulation results are listed in Table II.

MC simulations are compared to the RHNC and PT in Fig. 2 and Table II. The PT approximation gives the dielectric constant according to the relation²⁰

$$\epsilon - 1 = 3y + 3y^2 + 3y^3 p, \quad (11)$$

where

$$p = \frac{9I_{dd\Delta}}{16\pi^2} - 1$$

and $I_{dd\Delta}$ is the three-particle perturbation integral tabulated in Ref. 20(a). It is apparent that both the RHNC and the PT approximations are in good agreement with the MC results only for $(m^*)^2 < 2$. For higher polarities, the RHNC deviates upward and the PT downward from simulations. In the RHNC calculations of pure dipolar fluids in this section and in calculating the solute-solvent interaction energy in Sec. III B we used the basis of angular projections of the pair correlation function $h^{mn}(r)$ with $m, n \leq 2$. All our conclusions about the accuracy of the RHNC for pure liquids and solvation therefore refer only to this basis. Although the accuracy of the RHNC integral equations improves with increasing the basis set,²³ the feature of the RHNC to overemphasize dipolar correlations at high solvent polarities has been noticed by Wei *et al.*²⁴ also for a larger basis of angular projections $m, n \leq 4$.

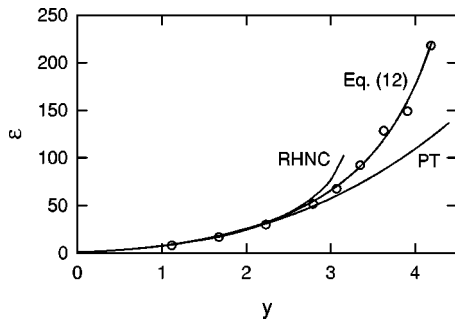


FIG. 2. ϵ vs y at $\rho^* = 0.8$. Points are the simulation results. Lines refer to the RHNC theory, perturbation theory of Tani *et al.* (PT, Ref. 20), and the interpolation equation (12).

The PT approximation is limited to relatively small y values by its construction. We found that better agreement with simulations is achieved by raising the three-particle term in Eq. (11) into the exponent

$$\epsilon - 1 = 3y + 3y^2 + \frac{2}{p^2} [\exp(3p^3 y^3 / 2) - 1], \quad (12)$$

as is illustrated in Fig. 2.

III. SOLVATION CHEMICAL POTENTIAL

In what follows we consider a single HS dipolar solute in a solvent of HS dipolar molecules. Since we are interested in excess thermodynamic properties, we can confine ourselves to the classical configurational partition functions for which we need to define only the potential energy of the system. The total potential energy, U , can be split into the solute-solvent, U_{0s} , and solvent-solvent, U_{ss} , parts (throughout below “0” stands for the solute and “s” for the solvent)

$$U = U_{0s} + U_{ss}. \quad (13)$$

For our dipolar solvation model, both U_{0s} and U_{ss} are given by sums of the HS repulsions and orientationally dependent dipole-dipole interactions

$$U_{0s} = U_{0s}^{\text{HS}} + U_{0s}^p, \quad U_{0s}^p = - \sum_j \mathbf{m}_0 \cdot \mathbf{T}_{0j} \cdot \mathbf{m}_j \quad (14)$$

and

$$U_{ss} = U_{ss}^{\text{HS}} + U_{ss}^p, \quad U_{ss}^p = - \frac{1}{2} \sum_{j \neq k} \mathbf{m}_j \cdot \mathbf{T}_{jk} \cdot \mathbf{m}_k. \quad (15)$$

Here \mathbf{m}_0 and \mathbf{m}_j are the dipole moments of the solute and the j th solvent molecule, respectively, and \mathbf{T}_{jk} is the usual dipole-dipole tensor $T_{jk}^{\alpha\beta} = \nabla_\alpha \nabla_\beta |\mathbf{r}_j - \mathbf{r}_k|^{-1}$. U_{0s}^{HS} and U_{ss}^{HS} stand for the HS repulsions.

We can determine the moments of the solute-solvent dipole-dipole interaction potential solely in terms of the solvation chemical potential. The connection is feasible through the generating functional

$$\mathcal{G}(x,z) = (Q_N)^{-1} \int \exp[-\beta x U_{0s}^p - \beta z U_{ss}^p - \beta U] d\Gamma_1^N \quad (16)$$

depending on the solute-solvent coupling parameter x and the solvent-solvent coupling z . The dependence on z is used in Sec. IV below to define mixed solute-solvent-solvent correlators. In Eq. (16), $d\Gamma_i$ is the differential of the center-of-mass positions and orientations of the i th molecule, $d\Gamma_1^N = d\Gamma_1 \dots d\Gamma_N$, and the partition function Q_N is for the N solvent molecules

$$Q_N = \int \exp[-\beta U_{ss}] d\Gamma_1^N.$$

For the dipolar interaction potential (13)–(15), the generating functional is expressed in terms of the chemical potential of solvation μ_p of an effective dipole \tilde{m}_0 in a dipolar liquid with the dipolar parameter \tilde{y} ,

$$\mathcal{G}(x,z) = \exp[-\beta \mu_p(\tilde{m}_0, \tilde{y})], \quad (17)$$

where

$$\tilde{m}_0 = m_0 \frac{1+x}{\sqrt{1+z}} \quad (18)$$

and

$$\tilde{y} = y(1+z). \quad (19)$$

The moments of the solute-solvent potential follow from the definition (16) and are given by derivatives of $\ln[\mathcal{G}(x,z)]$ with respect to the coupling parameter x . For the first two moments we have

$$\langle U_{0s}^p \rangle = \left. \frac{\partial \mu_p[\tilde{m}_0, \tilde{y}]}{\partial x} \right|_{x,z=0} \quad (20)$$

and

$$\langle (\delta U_{0s}^p)^2 \rangle = -\beta^{-1} \left. \frac{\partial \mu_p^2[\tilde{m}_0, \tilde{y}]}{\partial x^2} \right|_{x,z=0}, \quad (21)$$

where

$$\langle \dots \rangle = (Q_N)^{-1} \int \dots \exp[-\beta U] d\Gamma_1^N.$$

In the linear response approximation (LRA), the solute chemical potential is quadratic in m_0 , $\beta \mu_p = -am_0^2$, and we get two fundamental relations

$$e_{0s} = \langle U_{0s}^p \rangle = 2\mu_p \quad (22)$$

and

$$\beta \langle U_{0s}^p \rangle = -\beta^2 \langle (\delta U_{0s}^p)^2 \rangle. \quad (23)$$

The first and second moments of the solute-solvent potential are available from computer simulations and the extent of deviation from prediction (23) will be used below as a measure of nonlinear solvation. An analytical expression for the solute chemical potential including nonlinear solvation terms can be obtained by a Padé truncation of its perturbation expansion in powers of U_{0s}^p that we consider next.

A. Padé approximant

Padé approximation (PA) provides a way of truncating perturbation expansions for excess thermodynamic properties. It replaces a real perturbation expansion by a geometric series constructed from two leading perturbation terms. PA is not a self-consistent theory and several routes to obtain the solute chemical potential are possible. Stell and co-workers proposed to truncate the perturbation series for the free energy of homogeneous liquids.³ If this method is applied to solvation (μ route), we can get a Padé form of the chemical potential including terms nonlinear in m_0^2 [Eq. (1)]. Alternatively, we can truncate the perturbation expansion for the solute-solvent interaction energy $e_{0s} = \langle U_{0s}^p \rangle$ yielding (u route)

$$\beta e_{0s} = -\frac{2am_0^2}{1+4bm_0^2}. \quad (24)$$

The perturbation coefficients $a = a(y, \rho^*, \sigma, r_{0s})$ and $b = b(y, \rho^*, r_{0s})$ are functions of the solvent polarity, y , density, ρ^* , solvent HS diameter, σ , and the reduced distance of closest approach of the solute and solvent HS cores, $r_{0s} = R_0/\sigma + 0.5$. The linear response coefficient $a(y, \rho^*, r_{0s})$ reads

$$a = \frac{\beta}{R_{\text{eff}}^3} \frac{y}{1 + \kappa(\rho^*, r_{0s})y}. \quad (25)$$

Here R_{eff} represents the effective radius of a spherical dipolar solute²⁵

$$R_{\text{eff}}^{-3} = (3/\sigma^3) \int_0^\infty \frac{dx}{x^4} g_{0s}^{(0)}(x) \quad (26)$$

determined through the solute-solvent HS pair distribution function (PDF) $g_{0s}^{(0)}(r)$. For a low solvent density $\rho^* \rightarrow 0$, R_{eff} tends to $R_0 + \sigma/2$ that becomes equal to the solute radius R_0 in the continuum limit $\sigma \rightarrow 0$. At nonzero densities, due to effective packing of the solvent molecules in the first solvation shell, $R_{\text{eff}} < R_0 + \sigma/2$.

The parameter κ in Eq. (25) represents saturation of the dipolar solvent response due to angular correlations of the solvent permanent dipoles. In the PA κ is given by the ratio of the three-particle, $I_{0s}^{(3)}$, and two-particle, $I_{0s}^{(2)}$, perturbation integrals

$$\kappa(\rho^*, r_{0s}) = I_{0s}^{(3)}(\rho^*, r_{0s})/I_{0s}^{(2)}(\rho^*, r_{0s}). \quad (27)$$

$I_{0s}^{(2)}$ and $I_{0s}^{(3)}$ are tabulated in our previous publications.^{5(a),26}

The parameter $b(y, \rho^*, r_{0s})$ in Eq. (1) quantifies nonlinear saturation of orientations of the solvent permanent dipoles in the solute dipolar field. We determined it by the relation^{5(b)}

$$b(y, \rho^*, r_{0s}) = \frac{3\beta}{400\eta\sigma^3} \frac{yI_{0s}^{(4)}/I_{0s}^{(2)}}{(1+yI_{0s}^{(3)}/I_{0s}^{(2)})(1+yI_{0s}^{(5)}/I_{0s}^{(4)})}, \quad (28)$$

where $\eta = (\pi/6)\rho^*$ and the perturbation integrals $I_{0s}^{(4)}$ and $I_{0s}^{(5)}$ are given in Ref. 5(b).

The average solute-solvent interaction energy can be obtained from the chemical potential (1) according to Eq. (20),

$$\beta e_{0s}^{\mu} = -\frac{2am_0^2}{(1+bm_0^2)^2}, \quad (29)$$

where the superscript “ μ ” refers to the μ route. Similarly, the chemical potential derives from the u -route expression (24) in terms of the thermodynamic coupling parameter integration

$$\mu_p = \int_0^{m_0} \frac{d\lambda}{\lambda} \langle U_{0s}^p \rangle_{\lambda}, \quad (30)$$

resulting in

$$\beta\mu_p^u = -\frac{a}{4b} \ln[1+4bm_0^2]. \quad (31)$$

In Eq. (30), $\langle U_{0s}^p \rangle_{\lambda}$ refers to the solute with the dipole moment λ . Note also that throughout below brackets $\langle \dots \rangle$ without a subscript denote the infinite-size average over the solvent configurations in the field of the solute with the dipole m_0 .

Because of thermodynamic inconsistency of the PA, Eqs. (1) and (31) differ and, more importantly, have different types of dependence on the solute dipole moment. The u route predicts a stronger effect of nonlinear solvation on thermodynamic and spectroscopic properties. We show below that the ratio of the first and second moments of the solute-solvent potential provides a test of the impact of nonlinear solvation that favors the μ route. However, before testing the legitimacy of the Padé truncation as a method of evaluating the effect of nonlinear solvation, we first need to test the accuracy of the coefficients $a(y, \rho^*, \sigma, r_{0s})$ and $b(y, \rho^*, \sigma, r_{0s})$ to make sure that possible discrepancies between simulations and analytical results are rooted in the Padé method and not in the evaluation of the perturbation integrals in $a(y, \rho^*, \sigma, r_{0s})$ and $b(y, \rho^*, \sigma, r_{0s})$.

The perturbation integrals $I_{0s}^{(2)-(5)}$ were calculated^{5(a),5(b)} using HS PDFs obtained from the Verlet–Weis algorithm^{27(a)} in its extension to mixtures by Lee and Levesque.^{27(b)} This procedure relies on the off-diagonal contact value of the pair distribution function taken from the Boublik–Mansoori–Canahan–Starling–Leland equation of state.²⁸ The latter gives somewhat underestimated contact PDF values for large solutes²⁹ and this could cause an error in estimating the perturbation integrals. Another suspicious point is our use of the superposition approximation (SA) in calculating the three-particle integrals. Although the SA was found to be accurate for the evaluation of homogeneous three-particle integrals,^{20(a)} its performance may be worse for the asymmetric solute-solvent-solvent three-particle configuration. In order to test our previous tabulation of the perturbation integrals^{5(a),5(b)} we calculated them for configurations of the HS solvent around a HS solute obtained from MC simulations. The simulation details are given in the Appendix. Simulations are compared to calculations employing HS PDFs, combined with the SA for three-particle integrals, in Fig. 3. Taking into account inevitable errors of extrapolation used to obtain infinite-volume integrals from finite-volume simulated values (see the Appendix), the calculated and simulated perturbation integrals are in excellent agreement. Somewhat surprising is the good agreement between simu-

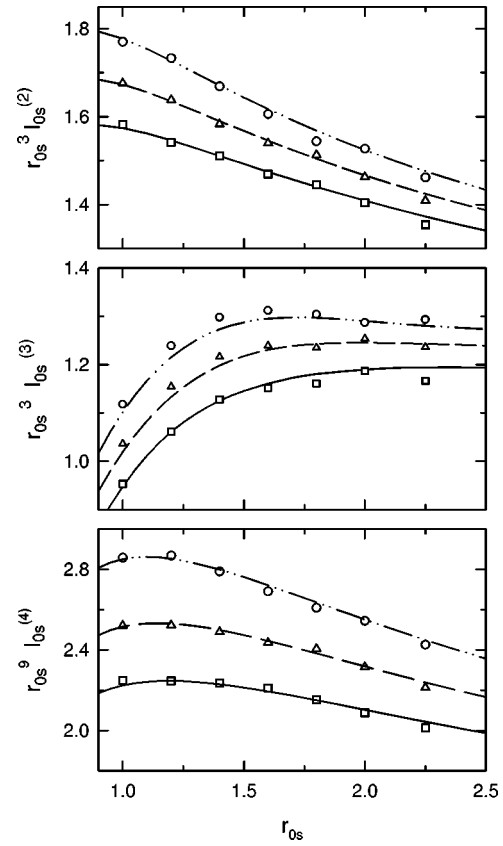


FIG. 3. Plots of $r_{0s}^3 \times I_{0s}^{(2)}$ (upper panel), $r_{0s}^3 \times I_{0s}^{(3)}$ (middle panel), and $r_{0s}^9 \times I_{0s}^{(4)}$ (lower panel) vs r_{0s} . Points and lines indicate, respectively, simulation results and calculations at $\rho^* = 0.9$ (circles, dash-dotted lines), $\rho^* = 0.8$ (triangles, dashed lines), and $\rho^* = 0.7$ (squares, solid lines). Calculations are carried out with the HS PDFs according to Verlet and Weis (Ref. 27).

lated and calculated three-particle integrals. The reason for that is the long-range character of the dipole-dipole interaction potential.^{20(a)} As a result, the bulk of the integrals comes from distances where the three molecules are well separated and the SA should be relatively accurate. (In fact, our calculations of three-particle integrals with more short-ranged potentials showed inapplicability of the SA in such cases.³⁰) Now, with the proven accuracy of the perturbation integrals involved in the chemical potential (1), we can proceed to testing the very method of Padé truncation for calculating the nonlinear chemical potential of dipole solvation.

B. Simulations of solvation thermodynamics

We carried out standard MC simulations in the canonical NVT ensemble of $N = 500$ solvent molecules. To create the initial configuration, the solute of the size 0.5σ was first inserted in the center of the fcc lattice of the solvent molecules. The solute size was then gradually increased to $r_{0s} = 1.4$ in the course of MC runs avoiding the solute-solvent overlap. The RF boundary conditions for the long-range dipole-dipole interactions with $\epsilon' = 1000$ and $R_c = L/2$ were employed. The average solute-solvent potential energy $\langle U_{0s}^p \rangle_V$, the second moment $\langle (\delta U_{0s}^p)^2 \rangle_V$, and the correlator $\langle \delta U_{0s}^p \delta U_{ss}^p \rangle_V$ (see Sec. IV below) were measured after the “aging” period of 50 000 cycles. Simulations were per-

TABLE III. $-\beta\langle U_{0s}\rangle_V$ (I) and $\beta^2\langle\delta U_{0s}^2\rangle_V$ (II) at $r_{0s}=1.4$ and $\rho^*=0.8$.

m_0/m	$(m^*)^2=1.0$			$(m^*)^2=2.0$			$(m^*)^2=3.0$	
	I	I ^a	II ^b	I	I ^a	II ^b	I	II ^b
2.0	2.35±0.08	2.32	2.28±0.06	5.88±0.04	5.70	5.8±0.2	9.83±0.02	
4.0	9.41±0.22	9.17	9.32±0.08	24.06±0.02	22.69	22.9±0.2	39.34±0.07	37.3±0.3
6.0	21.23±0.07	20.06	19.31±0.07	52.90±0.07	50.01	47.32±0.25	86.4±0.2	
7.0	29.52±0.10	26.53	26.15±0.07	71.78±0.08	65.86	66.34±0.12	118.6±0.2	109±2
8.0	35.89±0.05		32.86±0.14	92.40±0.15		80.8±0.4	151.7±0.1	132.2±1.4
9.0	45.60±0.04		39.8±0.2	114.2±0.1		97.4±0.6	188.8±0.1	153.8±1.2
10.0	55.51±0.07		45.96±0.09	139.9±0.1		106.4±0.4	231.3±0.2	

^aRHNC calculation. We could not achieve convergence of the iterative algorithm of solving the RHNC integral equations for $m_0/m > 7.0$ and $(m^*)^2 > 2.8$.

^bStandard deviation when the second moment achieves a stationary value. The error due to the finite system size may however be as large as 5%.

formed at different values of solvent polarity and for the range of solute dipole moments $2 \leq m_0/m \leq 10$. The first and second moments listed in Tables III–V, as well as their standard deviations, were measured by averaging over at least 50 000 cycles after all three moments had reached their stationary values. Usually, it took 250 000–350 000 cycles to get sufficiently long stationary plateaus. In some cases, especially at the highest polarity of $(m^*)^2 = 3.0$ studied, we could not reach stationary limits for the second moments. These cases correspond to blank entries in Tables III and V. Since ferroelectric phase transitions in soft³¹ and nonspherical hard³¹ dipolar fluids were reported in the literature, we have also monitored the heat capacity and ferroelectric order parameter^{2(c),31} during the simulation runs. No indication of a phase transition was found in the parameter range studied.

We also checked the dependence of the calculated values on the system size by running simulations with different numbers of solvent molecules: $N = 255$, 500, and 863 (Table VI). The first moment $\langle U_{0s}^p \rangle_V$ does not show any variation with the number of particles beyond simulation errors. $\langle (\delta U_{0s}^p)^2 \rangle_V$ varies up to 5% in going from $N = 255$ to $N = 500$, but there is no variation with changing from $N = 500$ to $N = 863$. The system size dependence is more pronounced for the moment $\langle \delta U_{0s}^p \delta U_{ss}^p \rangle_V$. However, also in this case, there is little change in the moment magnitude in passing from $N = 500$ to $N = 863$. We can therefore be confident that simulations with $N = 500$ solvent molecules can

give the finite-size moments within approximately 5% of their infinite-size values. The differences between Padé and simulated $\langle \delta U_{0s}^p \delta U_{ss}^p \rangle_V$ moments in Table V for large m_0/m ratios and solvent dipoles can be attributed to insufficiently long simulation runs. The solvent reorganization energy plotted against the number of simulation cycles shows relatively long plateaus which can be confused with final stationary values.

Figure 4 compares simulated (circles) and calculated (lines) solute-solvent energies e_{0s} depending on the solute dipole and solvent polarity. The solvation chemical potential (squares) was obtained by a polynomial extrapolation of the simulated e_{0s} energies used in the integration over the solute dipole moment in Eq. (30). The solute-solvent interaction energy e_{0s} from the μ route [Eq. (29), dashed lines] considerably exceeds simulations. Accordingly, the Padé chemical potential (1) deviates upward from the simulation results: For the highest solute dipole $m_0/m = 10$ and polarity $(m^*)^2 = 3.0$ studied the deviation amounts to 30%. The use of the u route [Eq. (24), dash-dotted lines] somewhat improves e_{0s} , but it is still too high. Also, from Table III, we see that the RHNC [basis of h^{mnl} with $m, n \leq 2$] somewhat ($\approx 8\%$) underestimates e_{0s} .³² Neither the PA, nor the RHNC thus give us accurate enough solutions for the solute-solvent interaction energy. Two questions arise in trying to improve the PA: (i) Which of the two routes of Padé truncation is preferable? (ii) Where is the main flaw of the PA

TABLE IV. Internal energy $-\beta\langle U_{0s}^p \rangle_V$ from simulations (MC) and the Padé approximation [PA, Eqs. (29) and (36)]; $\rho^* = 0.8$.

$(m^*)^2$	0.5	1.0	1.5	2.0	2.5	3.0	3.5	4.0
MC ^a	3.21	9.41	16.30	24.06	31.37	39.34	46.77	55.91
PA	3.19	9.21	16.21	23.66	31.36	39.21	46.83	55.17
MC ^b		2.04	3.67	5.51	7.43	9.49	11.6	
PA		1.99	3.62	5.40	7.27	9.20	11.2	
r_{0s} ^c	1.2	1.4	1.6	1.8				
MC	41.76	23.85	14.72	9.64				
PA	40.65	23.66	14.90	9.77				

^a $r_{0s} = 1.4$, $m_0/m = 4.0$.

^b $r_{0s} = 1.0$, $m_0/m = 1.0$.

^c $(m^*)^2 = 2.0$, $m_0/m = 4.0$.

TABLE V. $-\beta^2\langle\delta U_{0s}\delta U_{ss}\rangle_V$ at $r_{0s}=1.4$, $\rho^*=0.8$ from MC simulations (MC) and Padé approximation (PA).

m_0/m	$(m^*)^2$					
	1.0		2.0		3.0	
	MC	PA	MC	PA	MC	PA
2.0	1.25±0.09	1.27	5.2±0.2	4.2	5.0±0.2	7.8
4.0	5.23±0.06	5.0	16.3±0.2 ^a	16.4	31.9±0.7	30.1
6.0	10.3±0.2	10.9	35.5±1.2	35.3	74±3	64.2
7.0	15.1±0.2	14.5	44.5±0.3	46.6		84.4
8.0	20.0±0.4 ^a	18.4	58.4±0.9 ^a	58.8	103±2	106.0
9.0	21.3±0.1	22.7	68.4±0.9	71.6	114±2	128.2
10.0	25.4±0.2	27.2	77.3±1.7	84.7		150.5

^aWith $N = 863$ solvent molecules in the simulation box.

TABLE VI. System size dependence of the simulated moments; $r_{0s}=1.4$, $\rho^*=0.8$.

(m_0/m)	$(m^*)^2$	N	$-\beta\langle U_{0s}^p \rangle_V$	$\beta^2\langle \delta U_{0s}^2 \rangle_V$	$-\beta^2\langle \delta U_{0s} \delta U_{ss} \rangle_V$
4.0	2.0	255	23.78 ± 0.03	22.16 ± 0.15	12.6 ± 0.3
		500	24.06 ± 0.02	22.90 ± 0.20	16.2 ± 0.2
		863	23.75 ± 0.02	23.62 ± 0.13	16.3 ± 0.3
8.0	1.0	255	36.06 ± 0.05	28.48 ± 0.15	14.5 ± 0.4
		500	35.89 ± 0.05	32.86 ± 0.14	19.1 ± 0.3
		863	36.26 ± 0.07	31.69 ± 0.40	20.0 ± 0.4
8.0	2.0	255	92.77 ± 0.02	79.53 ± 0.46	42.9 ± 0.7
		500	92.34 ± 0.06	81.60 ± 0.50	56.1 ± 0.4
		863	92.40 ± 0.15	80.80 ± 0.40	58.4 ± 1.0

resulting in too high thermodynamic quantities? As we show below, the answers to these questions follow from examining the solute dipole and solvent polarity dependence of the two parameters

$$\chi_{NL} = -\beta \frac{\langle (\delta U_{0s}^p)^2 \rangle}{\langle U_{0s}^p \rangle} \quad (32)$$

and

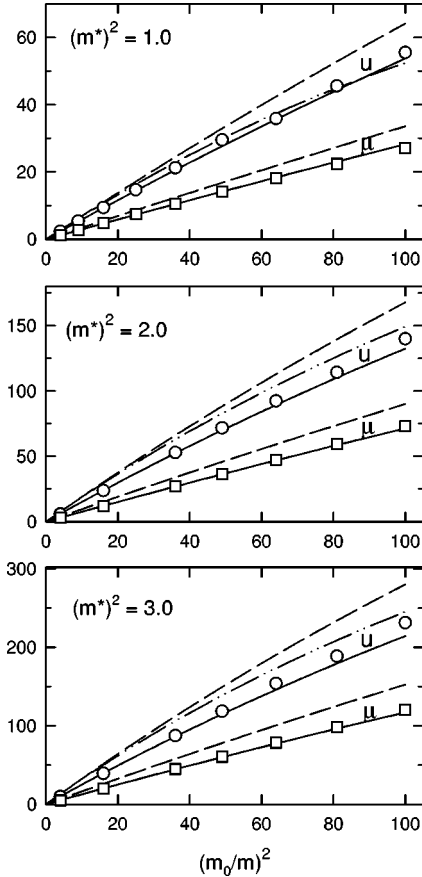


FIG. 4. The solute-solvent interaction energy e_{0s} (u) and solvation chemical potential (μ) vs $(m_0/m)^2$ at different solvent polarities. Lines indicate calculations with the Padé form in the μ route (dashed lines), u route (dash-dotted lines), and the μ route with corrected dipolar saturation factor κ [Eq. (36), solid lines]. The points are simulation results for e_{0s} (circles) and μ_p (squares).

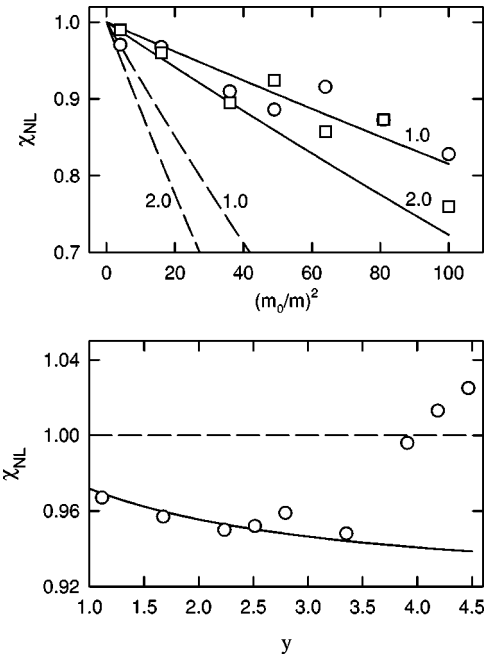


FIG. 5. The parameter of nonlinear solvation χ_{NL} calculated from the μ route (solid lines) and the u route (dashed lines) at $(m^*)^2$ equal to 1.0 and 2.0 (upper panel). The points are simulation results at $(m^*)^2=1.0$ (circles) and $(m^*)^2=2.0$ (squares). In the lower panel χ_{NL} vs y is shown for the fixed ratio $m_0/m=4.0$.

$$\chi_s = \beta \frac{\langle \delta U_{0s}^p \delta U_{ss}^p \rangle}{\langle U_{0s}^p \rangle}. \quad (33)$$

The nonlinear Padé form (1) is defined by the linear response coefficient a and the nonlinear solvation parameter b . We want to understand which of the two results is in major disagreement with the simulations. Let us first consider the ratio of the second and first moments of the solute-solvent dipole-dipole potential (32). The LRA predicts equality between the absolute values of the reduced first and second moments according to Eq. (23). Therefore, χ_{NL} serves as a measure of solvation nonlinearity. In the LRA, we have $\chi_{NL}=1$. The Padé approximation predicts that χ_{NL} is less than unity and is fully determined by the nonlinear solvation coefficient b and the magnitude of the solute dipole moment. We have from the μ route

$$\chi_{NL}^p = (1 - 3bm_0^2)/(1 + bm_0^2) \quad (34)$$

and

$$\chi_{NL}^p = (1 - 12bm_0^2)/(1 + 4bm_0^2) \quad (35)$$

from the u route.

In the upper panel in Fig. 5, we plotted χ_{NL} vs m_0/m from the μ route (solid lines) and u route (dashed lines) as well as from simulations (points). As is seen, the u route predicts too strong a nonlinear effect compared to simulations. The simulation points, although scattered, are closer to the prediction of the μ route for $(m^*)^2=1.0, 2.0$. As is seen in the lower panel in Fig. 5, this agreement extends up to $y \approx 3.5$ for $m_0/m=4.0$. For higher y values, χ_{NL} deviates upward from the decaying trend predicted by the PA and becomes even larger than unity. In Sec. V, we explain this

phenomenon in terms of switching the nonlinear solvation mechanism from orientational saturation described by the PA to electrostriction. Electrostriction is not accounted for by the Padé form (1) that is the reason for the observed disagreement.

Next, we want to improve the numerical accuracy of the PA. The dependence of the parameter χ_s [Eq. (33)] on y considered in Sec. IV (Fig. 7) shows explicitly that it is the linear response coefficient a that primarily needs correction. In Eq. (25), the term $\beta y/R_{\text{eff}}^3$ corresponds to the low-polarity perturbation expansion of μ_p that is exact for small y . The main approximation of the PA is involved in the estimate of the saturation parameter κ (27) as the ratio of two perturbation integrals. We will therefore seek an improvement of the PA in changing κ . The correction

$$\kappa = [1 + (1 - 1/2r_{0s})^2] I_{0s}^{(3)}/I_{0s}^{(2)} \quad (36)$$

substantially improves the agreement between simulations and the PA (the solid lines in Fig. 4). As is shown in Table IV, both the dependence on y and the solute size of simulated e_{0s} conform with the PA (1) within 3% when Eq. (36) is used in the linear response coefficient a [Eq. (25)]. Although the correction factor in Eq. (36) is a totally empirical one, we have chosen it to obey the limit of a macroscopic solute in a highly polar solvent with $y \rightarrow \infty$. In this case, the macroscopic Onsager theory³³ with

$$a^O(y) = \frac{\beta}{R_{\text{cav}}^3} \frac{\varepsilon(y) - 1}{2\varepsilon(y) + 1} \quad (37)$$

predicts $a^O \rightarrow \beta/2R_0^3$ (the superscript ‘‘O’’ labels the Onsager reaction-field theory). The PA with κ from Eq. (36) gives $a \rightarrow (\beta/2R_{\text{eff}}^3)(I_{0s}^{(2)}/I_{0s}^{(3)})$. In the limit $R_0/\sigma \gg 1$ we have $R_{\text{eff}} \rightarrow R_0 \approx R_{\text{cav}}$ and the ratio of the perturbation integrals is very close to unity thus recovering the macroscopic Onsager limit.

With accurate simulation data for both the solvation thermodynamics and homogeneous dielectric properties of the solvent we can now test the cavity concept of dielectric continuum theories of dipole solvation. Continuum theories are based on the LRA and, according to Eq. (22), the solute-solvent interaction energy is

$$\beta e_{0s} = -2a^O(y)m_0^2. \quad (38)$$

The assumption explicitly or implicitly made in all continuum treatments is that, as long as the cavity radius is defined, Eqs. (37) and (38) give a correct solvent polarity variation of the solvation thermodynamic potentials. Figure 6 shows cavity radii obtained at different y by fitting Eqs. (37) and (38), with the dielectric constants calculated in Sec. II, to the RHNC (the solid line) and simulated (points) solute-solvent interaction energies e_{0s} . The horizontal reference lines indicate the solute radius R_0 , the distance of the closest solute-solvent approach $R_0 + \sigma/2$, and the effective radius R_{eff} of the perturbation theory. Since it is used in numerous applications,³⁴ for comparison, we also showed the effective radius of ion solvation in the framework of the mean spherical approximation (MSA)

$$R_{\text{eff}}^{\text{MSA}}/\sigma = r_{0s} - \Lambda_p/\sigma. \quad (39)$$

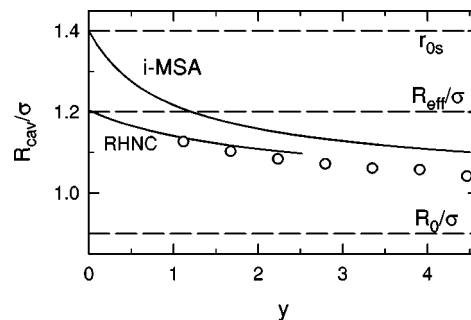


FIG. 6. The cavity radius obtained by fitting the Onsager solute-solvent interaction energy [Eqs. (37) and (38)] to simulations (points) and the RHNC theory vs the dipolar polarity parameter y . The dielectric constant at $(m^*)^2 = 4.0$ is obtained from Eq. (12). Also shown is the MSA effective radius of ion solvation [*i*-MSA, Eq. (39)]. The dashed reference lines indicate the solute radius R_0 , the effective radius R_{eff} [Eq. (26)], and the closest approach distance $R_0 + \sigma/2$.

Here Λ_p is the length of longitudinal correlations of the permanent dipoles in the pure solvent, $\Lambda_p/\sigma = 3\xi/(1 + 4\xi)$,³⁵ ξ is the MSA solvent polarity parameter.¹⁶

Both the RHNC theory and MC simulations lead to a significant dependence of the cavity radius on y . There is, therefore, no unique cavity radius for a given solute. Already this makes continuum theories inapplicable for analyzing solvation data over a wide polarity range. The solvent dependence of the cavity radius gets smoother at high y and the problem may seem insignificant rendering the cavity size an adjustable parameter in every solvent. The dipolar response contains, however, a very strong cubic dependence on R_{cav} resulting in further inconsistencies of the continuum picture. For HS dipolar fluids, the temperature comes explicitly only into the polarity parameter y : a dependence on y means also a dependence on temperature. Therefore, a cavity radius fitted to the solvation chemical potential at some temperature cannot be used at other temperatures. This also implies that continuum models cannot be employed for splitting the chemical potential into the internal energy and entropy, as we explicitly show in Sec. IV. As mentioned in Sec. I, in our dipolar fluid model, the peak of the solute-solvent distribution function is always fixed at $R_0 + \sigma/2$. This distance is solvent independent and, as seen in Fig. 6, greatly exceeds the fitted cavity radius. Hence, the location of the first peak of the spherically symmetric solute-solvent PDF cannot be used as a cavity radius, as sometimes proposed.^{9,36}

IV. SOLVATION INTERNAL ENERGY

The internal energy of dipole solvation e_p is a temperature derivative of the chemical potential (30) resulting in the fundamental relation³⁷

$$e_p = e_{0s} + e_{ss}. \quad (40)$$

It includes the average solute-solvent interaction energy e_{0s} and the change in the solvent-solvent interaction energy (with respect to the bulk solvent) induced by the solute^{37(b)}

$$e_{ss} = -\beta \int_0^{m_0} \frac{d\lambda}{\lambda} \langle \delta U_{0s}^p \delta U_{ss}^p \rangle_\lambda. \quad (41)$$

Here $\delta U_{0s}^p = U_{0s}^p - \langle U_{0s}^p \rangle_\lambda$, $\delta U_{ss}^p = U_{ss}^p - \langle U_{ss}^p \rangle_\lambda$ and, as above, the subscript λ refers to a solute with the dipole moment equal to λ . From Eqs. (17) to (19), we get

$$\langle \delta U_{0s}^p \delta U_{ss}^p \rangle = -\beta^{-1} \left. \frac{\partial^2 \mu_p(\bar{m}_0, \bar{y})}{\partial x \partial z} \right|_{x,z=0}. \quad (42)$$

General relations for the e_{0s} and e_{ss} solvation energies are available in the LRA when the solvation chemical potential is quadratic in m_0 : $\beta \mu_p = -a(y)m_0^2$. In this case,

$$\beta e_{0s} = -2a(y)m_0^2$$

and

$$e_{ss} = -(\beta/2) \langle \delta U_{0s}^p \delta U_{ss}^p \rangle.$$

Also, from Eq. (42), we have

$$e_{ss} = -e_{0s} \left(1 - y \frac{\partial \ln a(y)}{\partial y} \right). \quad (43)$$

Equation (43) is an important result based solely on the thermodynamic derivation and hence valid for any linear response theory. It gives us a convenient tool of calculating the solvent-solvent component of the solvation energy. It appears that the knowledge of the solute-solvent response coefficient $a(y)$ suffices to get e_{ss} . For instance, we can obtain e_{ss} for a continuum solvation model that, in fact, does not specify the nature of the solvent-solvent interactions in the liquid replacing it by a dielectric continuum. Further, all the terms independent of solvent polarity disappear from the logarithmic derivative in Eq. (43). This implies, for example, that the solvent independent cavity term of continuum theories does not affect the magnitude of the factor in brackets in Eq. (43). The parameter χ_s defined by Eq. (33) reads in the LRA

$$\chi_s = -\frac{2e_{ss}}{e_{0s}} = 1 - y \frac{\partial \ln a(y)}{\partial y}. \quad (44)$$

χ_s may serve as an indicator of the ability of a linear response theory to predict the solvent dependence of the response function irrespective of the procedure used to determine the solute (cavity) size as long as the latter is independent of the solvent dipole moment.

For the Onsager response function (37) we can get χ_s from the Kirkwood connection (4) of the solvent dielectric constant to the solvent polarity parameter y . This yields

$$\chi_s = 1 - \frac{3\varepsilon}{2\varepsilon^2 + 1} \frac{\partial \ln(yg_K(y))}{\partial y}. \quad (45)$$

For the linear response Padé form [$b=0$, Eq. (25)] we get

$$\chi_s = \frac{\kappa y}{1 + \kappa y}. \quad (46)$$

The moment $\langle \delta U_{0s}^p \delta U_{ss}^p \rangle$ for the nonlinear Padé form (1) follows from Eq. (42) yielding

$$\beta \langle \delta U_{0s}^p \delta U_{ss}^p \rangle = \langle U_{0s}^p \rangle \frac{\kappa y}{1 + \kappa y} \frac{1 - bm_0^2}{1 + bm_0^2}. \quad (47)$$

In deriving Eq. (47) we used the approximation $b(y) \propto y$ neglecting the y dependence of $b(y)$ originating from the Padé

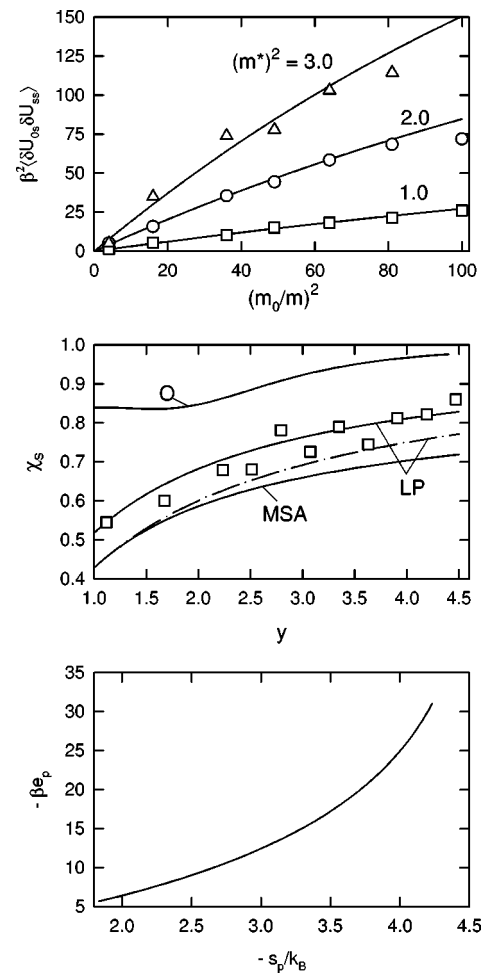


FIG. 7. Upper panel: $\beta^2 \langle \delta U_{0s}^p \delta U_{ss}^p \rangle$ vs $(m_0/m)^2$ at different solvent polarities: $(m^*)^2 = 1.0$ (squares), $(m^*)^2 = 2.0$ (circles), $(m^*)^2 = 3.0$ (triangles). Points are simulation results and solid lines are according to Eq. (47). Middle panel: the parameter χ_s [Eq. (33)] vs y from the continuum Onsager theory ("O"), linear Padé theory [LP, Eq. (46)], and the MSA at $m_0/m = 4.0$, $r_{0s} = 1.4$, and $\rho^* = 0.8$. For the LP, the dash-dotted line indicates the Padé solution without correction (36) and the solid line with the correction included. Lower panel: e_p vs s_p at different y values and $m_0/m = 4.0$. Points are simulation results.

truncation of the solvent dependence of the $\propto m_0^4$ nonlinear solvation term. Differentiation of the Padé form with respect to the solvent polarity parameter y may lead to erroneous results as indeed happens concerning the derivative $\partial b(y)/\partial y$. The Padé chemical potential is an approximation and all the thermodynamic properties derived from it must be tested against simulations. As is shown in the upper panel in Fig. 7, the moment $\langle \delta U_{0s}^p \delta U_{ss}^p \rangle$ given by Eq. (47) is indeed in a fairly good agreement with simulations for $(m^*)^2 = 1.0$ and 2.0 when the internal energy e_{0s}^μ with the corrected linear response coefficient a [Eqs. (25) and (36)] is substituted into Eq. (47). The values for $(m^*)^2 = 3.0$ in the upper panel in Fig. 7 are more scattered reflecting the general trend of declining the simulation's accuracy with increasing y .

In the middle panel in Fig. 7, we show χ_s vs y calculated from the Onsager continuum response [Eq. (45), "O" in Fig. 7], the linear Padé form [Eq. (46), "LP" in Fig. 7], and simulations (points). The points in Fig. 7 were obtained from simulated averages $\langle U_{0s}^p \rangle_V$ after correcting for solvation non-

linearity according to Eq. (34). There is generally a good agreement between the Padé and simulation results in the whole polarity range lending additional support to the linear response coefficient given by Eqs. (25) and (36). Figure 7 also shows the parameter χ_s calculated in the framework of the mean spherical approximation (MSA) for dipolar HS mixtures (“MSA” in Fig. 7).^{5(a),38}

One interesting feature of the solvent-solvent contribution to the solvation thermodynamics is the exact compensation of the internal energy, e_{ss} , and entropy, Ts_{ss} , contributions in the solvation chemical potential. The chemical potential does not depend on the solute-induced change in the solvent structure near the solute because of the thermodynamic equality^{37(b),39}

$$e_{ss} = Ts_{ss}.$$

This equation was claimed to be responsible for the existence of isokinetic relationships that are defined as a linear relation between the entropy and internal energy⁴⁰ changes for some process (reaction, solvation, etc.) when some parameter (e.g., the solvent) is varied.^{37(c)} In fact, for linear solvation, we can indeed write down a relation between the energy e_p and entropy s_p of solvation. We have

$$e_p = e_{0s} + e_{ss} = e_{0s}(1 - \chi_s/2)$$

and

$$Ts_p = \frac{1}{2}e_{0s} + Ts_{ss} = (e_{0s}/2)(1 - \chi_s).$$

Therefore, we get

$$e_p = Ts_p \frac{2 - \chi_s}{1 - \chi_s}. \quad (48)$$

Because the factor χ_s depends on solvent polarity, there is no universal relationship between e_p and s_p . However, the dependence of χ_s on y is relatively weak (the middle panel in Fig. 7) and in a narrow range of solvent polarities a linear isokinetic trend may indeed be observed. We still need to stress that such a trend does not reflect any fundamental connection between the internal energy and the entropy and is merely a reflection of the fact that the ratio of e_{ss} and e_{0s} varies smoothly with solvent polarity (Fig. 7, lower panel).

Equation (48) also gives us the relative weights of the internal energy and entropy in the solvation chemical potential. From the middle panel in Fig. 7 we see that, in dielectric continuum theories, χ_s is close to unity and the internal energy is the main component of μ_p . χ_s is much smaller in molecular treatments (both in the MSA and Padé) resulting in a larger entropic component in the solvation free energy.

V. DISCUSSION

The preceding development concerned chiefly the quantitative aspects of dipole solvation thermodynamics. In this section, we give some qualitative insights that can be gained from our calculations. In order to provide better understanding of major components of the solvent response, we build our discussion on a simplified, but physically transparent, derivation of the solvation chemical potential.

The interaction energy of a solvent dipole $\langle \mathbf{m} \rangle_{E_0}$ in equilibrium with the solute field $\mathbf{E}_0(\mathbf{r})$ at point \mathbf{r} reads

$$u_{E_0}(\mathbf{r}) = -\langle \mathbf{m} \rangle_{E_0} \cdot \mathbf{E}_0(\mathbf{r}).$$

The chemical potential of solvation can then be obtained from thermodynamic integration over the solute field as follows:

$$\mu_p = \rho \int d\mathbf{r} \int_0^{E_0} d\mathbf{E} \cdot \langle \mathbf{m} \rangle_E. \quad (49)$$

The average solvent dipole $\langle \mathbf{m} \rangle_E$ is given, in the mean-field approximation, by a Langevin function and if only the first nonvanishing term in the expansion of $\langle \mathbf{m} \rangle_E$ over the solute field E (the superscript “1,” LRA) is taken, we get^{10(a)}

$$u_{E_0}^{(1)}(\mathbf{r}) = -\frac{3\varepsilon}{2\varepsilon+1} \frac{\beta m^2}{3} E_0(\mathbf{r})^2 \quad (50)$$

and

$$\mu_p^{(1)} = -\frac{9y\varepsilon}{2\varepsilon+1} \frac{1}{8\pi} \int E_0(\mathbf{r})^2 d\mathbf{r}. \quad (51)$$

Here, the cavity field factor $3\varepsilon/(2\varepsilon+1)$ accounts for the difference between the effective solvent dipole moment in a dielectric continuum and in the vacuum.^{10(a),33}

Equations (50) and (51) correspond to a one-particle solvent response, i.e., a change in the orientation of any particular solvent molecule is assumed to be independent of the surrounding solvent dipoles. In fact, this is a very poor approximation for dense polar fluids. Because of the long range of dipolar forces, the orientations of solvent dipoles are strongly correlated and the orientational response has a many-body character. To account for screening by the surrounding dipoles, we need to multiply the one-particle response by a screening response function. Actually, the situation is not as simple and, to account for the nonlocal feature of dipolar correlations, we need to write down an integral of the product of interaction potentials taken at points \mathbf{r}_1 and \mathbf{r}_2 convoluted with a response function depending on $\mathbf{r}_1 - \mathbf{r}_2$. The convolution is simplified in Fourier \mathbf{k} space. If the solute is large compared to the solvent molecules, the Fourier transform of the response function can be approximated by its $k=0$ value and Eq. (51) reads

$$\mu_p^{(1)} = -\frac{9y\varepsilon}{2\varepsilon+1} \frac{S(0)}{8\pi} \int E_0(\mathbf{r})^2 d\mathbf{r}, \quad (52)$$

where $S(0)$ refers to the Fourier transform of the dipolar response function at $k=0$. When the longitudinal response function

$$S(0) = (3y)^{-1}(1 - 1/\varepsilon), \quad (53)$$

and the dipolar solute field (with the cutoff at the cavity radius R_{cav}) are used in Eq. (52), we come to the Onsager result for the solvation chemical potential

$$\mu_p^{(1)} = -\frac{m_0^2}{R_{\text{cav}}^3} \frac{\varepsilon - 1}{2\varepsilon + 1}. \quad (54)$$

For solutes not much larger than solvent molecules, the $k=0$ approximation for the dipolar response function is not

accurate necessitating a dependence of the cavity radius on solvent polarity discussed in Sec. III B. This complication that may seem to be only a quantitative problem results in a fundamental failure of continuum models to predict energies and entropies of dipole solvation, as we explicitly showed in Sec. III. The same flaw was found for ion solvation.^{8(b)} This enables us to suggest that continuum theories must be generally restricted to the chemical potential in treating multipole solvation.

In deriving the solvation chemical potential according to Eq. (49) we explicitly assumed that all the positions of a probe solvent molecule around the solute are equivalent. This is a reasonable approximation only for large solutes. For solutes and solvents of comparable sizes we need to take into account packing effects resulting in preference of one position of a solvent molecule over another. This feature is represented by the spherically symmetric projection $g_{0s}^{(0)}(r)$ of the solute-solvent PDF. Equation (49) thus transforms to

$$\mu_p = \rho \int g_{0s}^{(0)}(r) d\mathbf{r} \int_0^{E_0} d\mathbf{E} \cdot \langle \mathbf{m} \rangle_E.$$

If we continued the derivation as is done above, we would come to Eq. (54) with the effective radius R_{eff} [Eq. (26)] instead of R_{cav} . The problem that arises in pursuing this approach is that the local solute-solvent structure affects also the screening function of the solvent dipoles. In contrast to the long-ranged dipolar forces, packing produces a short-ranged structure and the $k=0$ value can be taken only for the orientational part of the response. As a crude approximation we thus get⁴¹

$$\mu_p^{(1)} = -\frac{m_0^2}{R_1^3} \frac{\varepsilon - 1}{2\varepsilon + 1} + \delta\mu_p^{(1)}, \quad (55)$$

where

$$\delta\mu_p^{(1)} = -\frac{9y\varepsilon m_0^2}{2\varepsilon + 1} \int_0^\infty \frac{dr}{r^4} \theta(r - R_1) h_{0s}^{(0)}(r), \quad (56)$$

$R_1 = R_0 + \sigma/2$, $h_{0s}^{(0)}(r) = g_{0s}^{(0)}(r) - 1$, and $\theta(x)$ is a step function.

The solute-solvent correlation function $h_{0s}^{(0)}(r)$ in Eq. (56) can be expressed through the corresponding solvent-solvent correlation function $h_{ss}^{(0)}(r)$ by using the Ornstein-Zernike equation

$$\theta(r - R_1) h_{0s}^{(0)}(\mathbf{r}) = \theta(r - R_1) \rho \int c_{0s}^{(0)}(\mathbf{r}') h_{ss}^{(0)}(\mathbf{r}' - \mathbf{r}) d\mathbf{r}',$$

where $c_{0s}^{(0)}(\mathbf{r})$ is the solute-solvent direct correlation function and, for hard spheres, $\theta(r - R_1) c_{0s}^{(0)}(\mathbf{r}) = 0$. The function $\rho h_{ss}^{(0)}(\mathbf{r})$ reflects correlations between density fluctuations in the homogeneous solvent. Therefore, the term $\delta\mu_p^{(1)}$ in Eq. (55) can be interpreted as an enhancement of the solvation free energy due to fluctuations of the solvent density around its equilibrium value. (The corresponding solvation term in the reorganization energy of electron transfer reactions was termed the density reorganization energy.⁴¹) This contribu-

tion comes to the linear response term. The change in the *equilibrium local* density compared to its bulk value caused by the solute field is, however, a purely nonlinear effect termed electrostriction in dielectric theories.¹⁰

In our simplified derivation, we can account for electrostriction by including the distance-dependent density variation $\Delta\rho(E)$ into the solvation chemical potential

$$\mu_p^e = S(0) \int d\mathbf{r} \int_0^{E_0} d\mathbf{E} \cdot \langle \mathbf{m} \rangle_E \Delta\rho(E). \quad (57)$$

In the continuum representation of the solvent, the following relation holds for $\Delta\rho(E)$:^{10(a)}

$$\Delta\rho(E) = \beta_T \rho^2 \left(\frac{\partial \varepsilon}{\partial \rho} \right)_T \frac{E(r)^2}{8\pi}, \quad (58)$$

where β_T is the isothermal compressibility of the homogeneous solvent. From Eqs. (53), (57), and (58) we get

$$\mu_p^e = -\frac{\beta_T \rho}{20\pi} \left(\frac{\partial \varepsilon}{\partial \rho} \right)_T \frac{\varepsilon - 1}{2\varepsilon + 1} \frac{m_0^4}{R_1^9}. \quad (59)$$

Electrostriction hence produces a negative contribution to the solvation chemical potential enhancing its absolute value. Conversely, orientational saturation diminishes solvation stabilization. The second-order term (the superscript ‘‘2’’) of the Langevin function representing the average solute dipole $\langle \mathbf{m} \rangle_E$ gives for the corresponding interaction energy term^{10(a)}

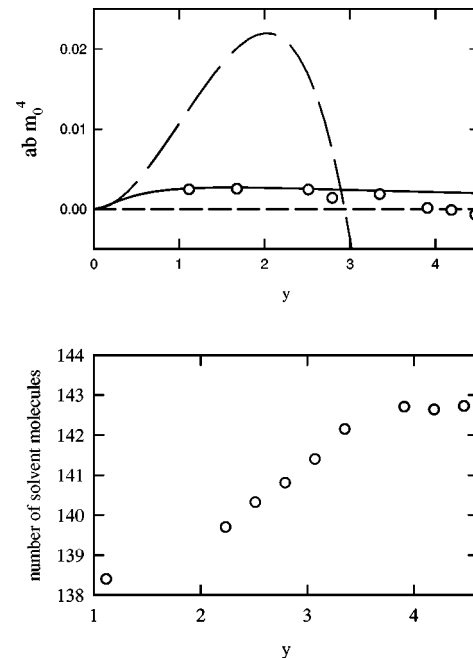


FIG. 8. The nonlinear $\propto m_0^4$ expansion coefficient obtained as $\mu_p^e + \mu_p^{(2)}$ (dashed line) and from the expansion of the Padé form, abm_0^4 , with b from Eq. (28) (the solid line) and from simulations (points) according to Eq. (34). In the lower panel, numbers of solvent molecules in the shell $1.4 \leq r/\sigma \leq 2.4$ from the simulations are shown at different y ; $m_0/m = 4.0$, $r_{0s} = 1.4$, $\rho^* = 0.8$.

TABLE VII. Solvation moments and parameters χ_{NL} and χ_s from MC simulations at $m_0/m=4.0$, $r_{0s}=1.4$, and $\rho^*=0.8$.

Parameter	$(m^*)^2$								
	1.0	1.5	2.0	2.25	2.5	3.0	3.5	3.75	4.0
$-\beta\langle U_{0s}^p \rangle_V$	9.4	16.3	24.1	27.6	31.7	39.3	47.2	51.2	55.9
$\beta^2\langle (\delta U_{0s}^p)^2 \rangle_V$	9.1	15.6	22.9	26.3	30.4	37.3	47.0	51.4	57.3
$-\beta^2\langle \delta U_{0s}^p \delta U_{ss}^p \rangle_V$	5.2	10.0	16.8	19.2	24.8	31.9	38.4	42.0	47.5
χ_{NL}	0.967	0.957	0.950	0.952	0.959	0.948	0.996	1.004	1.025
χ_s	0.545	0.600	0.679	0.680	0.770	0.790	0.812	0.822	0.861

$$\mu_E^{(2)}(\mathbf{r}) = \frac{\beta^3 m^4}{45} \left(\frac{3\varepsilon}{2\varepsilon+1} \right)^3 E_0(\mathbf{r})^4$$

and, for the solvation chemical potential,

$$\mu_p^{(2)} = \frac{6\beta^2 m^2 \varepsilon^2 (\varepsilon-1) m_0^4}{25 (2\varepsilon+1)^3 R_1^9}. \quad (60)$$

Calculations using the RHNC compressibility in Eq. (59) show that the two nonlinear terms, μ_p^e and $\mu_p^{(2)}$, are very close in absolute value, but have opposite signs. Their sum is about an order of magnitude smaller than each component resulting in compensation of nonlinear saturation by electrostriction. This effect, well-known for ion solvation,^{8(a),8(d)} is the reason for a small nonlinear solvation effect in liquids compared to solids where rigid structure suppresses electrostriction.⁴² In Fig. 8, we compared $\mu_p^e + \mu_p^{(2)}$ (the dashed line) to the expansion term abm_0^4 with a taken from the improved Padé form [Eqs. (25) and (36)] and b from Eq. (28) (the solid line) and from simulations (points) according to Eq. (34). Because of the continuum dielectric assumption and a crude estimate of dipolar screening effects, the compensation in $\mu_p^e + \mu_p^{(2)}$ is not exact leading to a substantial deviation from perturbation and simulation results. Our aim in this section was not to give a rigorous treatment, but to gain clear physical insights into mechanisms of nonlinear solvation. The simplified derivation performed above meets this goal showing that the sign switch of the nonlinear $\propto m_0^4$ term is due to a competition between orientational saturation and electrostriction: Orientational saturation prevails at low y and electrostriction becomes the dominant factor at higher polarities.

In order to test a possibility of switch in the nonlinear solvation mechanism, we performed simulations for the constant ratio $m_0/m=4.0$ at different y . The simulation results are listed in Table VII and are shown by points in Figs. 5 and 8. Although scattered, the simulated values of the b coefficient obtained using Eq. (34) seem to support the change of the nonlinear solvation mechanism from saturation to electrostriction. This change is concomitant with the increase in the solvent density in the solute vicinity, as is illustrated in the lower panel in Fig. 8. The switch of the nonlinear solvation mechanism is reflected by a very nontrivial behavior of the nonlinear solvation parameter (32) with dipolar strength

y . As is seen in the lower panel in Fig. 5 and Table VII, χ_{NL} is less than unity following the Padé prediction in the range $0 < y < 3.5$. It becomes however larger than unity at higher y implying that electrostriction makes the solvent fluctuate even stronger than the LRA would predict. We should stress, however, that the nonmonotonic behavior of the nonlinear parameter as a function of solvent polarity was obtained for a constant ratio of the solute and solvent dipole moments. Thus, an increase in the solvent dipolar strength was accompanied by strengthening the solute solvation power. Such a situation is hardly realizable in experiment where changing of the solvent for a particular solute is the common strategy of studying solvation. In such cases, most probably, only the orientational saturation regime well described by the Padé approximation will be observed. Note also that in real liquids the dipolar correlations are effectively destroyed by molecular quadrupoles^{16,43} and the electrostriction regime of nonlinear solvation may not be attainable. This problem needs further investigation involving model liquids with higher multipoles.

As we have shown in Sec. IV, the parameter χ_s may serve as a test of how adequately a particular linear response theory gives the dependence of the solvent response on solvent polarity. Figure 7 shows that the Onsager theory does a very poor job in predicting χ_s . The inaccurate estimate of χ_s results in a wrong splitting of the solvation free energy into the internal energy and entropy of solvation [Eq. (48)]. The equilibrium solvation energy, e_p , and the entropy, s_p , are formed as sums of negative solute-solvent stabilization parts and positive solvent-solvent contributions. For e_p the solute-solvent part accounts for about 60%–70% of the total solvation energy. By contrast, the two components in the entropy are very close in magnitude and the solvation entropy is always substantially smaller than the solvation energy (in absolute value, see Fig. 7). This situation is very different from the thermodynamics of solvent effects on optical transitions. In the latter case, the solvent-solvent part of solvation remains constant for a Franck-Condon transition and cancels out (apart from a small polarizability effect⁴⁴) in the spectral shift.

ACKNOWLEDGMENT

This work was supported by the National Science Foundation Grant No. CHE-9520619.

TABLE VIII. Perturbation integrals calculated on HS configurations from MC simulations.

r_{0s}	$r_{0s}^3 \times I_{0s}^{(2)}$			$r_{0s}^3 \times I_{0s}^{(3)}$			$r_{0s}^9 \times I_{0s}^{(4)}$			$r_{0s}^9 \times I_{0s}^{(5)}$		
	$\rho^*=0.7$	0.8	0.9	$\rho^*=0.7$	0.8	0.9	$\rho^*=0.7$	0.8	0.9	$\rho^*=0.7$	0.8	0.9
1.0	1.596	1.676	1.796	0.953	1.036	1.118	2.281	2.529	2.881	3.890	4.650	5.645
1.2	1.571	1.634	1.796	1.061	1.152	1.240	2.245	2.522	2.881	3.913	4.674	5.639
1.4	1.511	1.584	1.670	1.128	1.216	1.298	2.234	2.489	2.789	3.510	4.126	4.849
1.6	1.470	1.540	1.670	1.153	1.239	1.298	2.211	2.436	2.789	2.912	3.358	3.936
1.8	1.445	1.513	1.544	1.189	1.236	1.304	2.153	2.405	2.609	2.343	2.633	2.830
2.0	1.404	1.463	1.527	1.187	1.254	1.287	2.088	2.315	2.544	1.647	1.876	2.115
2.25	1.354	1.409	1.462	1.166	1.236	1.293	2.014	2.213	2.425	0.733	0.869	0.944

APPENDIX: PERTURBATION INTEGRALS

Here we describe the calculation of the perturbation integrals needed to determine the Padé chemical potential. The integrals are evaluated for configurations of the HS solvent generated by MC simulations done by the Metropolis method.^{2(c)} HS solutes of different sizes were placed in the center of the simulation box and held fixed during the simulation runs. In the starting configuration a solute of radius $\sigma_0=0.5\sigma$ was placed in the center of the cubic simulation box with the fcc lattice formed by the solvent molecules and then its size was gradually increased in standard MC runs. The simulations were performed for $N=108, 255,$ and 500 solvent molecules in the box. (In the initial fcc configuration containing 256 particles the center of a solvent molecule coincides with the center of the simulation cell. In this configuration, the solute was first identified with this HS molecule and then its size was increased to the desired magnitude.) Typical MC calculations consisted of an equilibration period of $(10-20) \times 10^6$ configurations followed by production runs of about $(90-100) \times 10^6$ moves. The convergence was monitored by measuring the perturbation integrals and the contact value of the solute-solvent PDF^{2(c)} that is the most slowly converging property.²⁹

We found all integrals to depend on the number of the solvent molecules in the simulation box. The variation with the system size is most pronounced for $I_{0s}^{(3)}$ as illustrated in Fig. 3. Two reasons contribute to the dependence on the system size. First, for finite simulation systems, the integrals were cut at distance $L/2$ for a cubic simulation box with the side length L . The cutoff results in underestimation of the integrals, especially of the long-range three-particle integral $I_{0s}^{(3)}$, as was previously noticed by Tani *et al.*^{20(a)} The second reason is more trivial. The reduced density for our simulation conditions is given by the relation

$$\rho^* = \rho_1^* (1 + d^3/N), \quad \rho_1^* = (N/V)\sigma^3,$$

where V is the simulation cell volume. Therefore, the effective solvent density in the simulations is lower by d^3/N than its infinite dilution value. In order to obtain true infinite dilution results the perturbation integrals obtained at three solute concentrations $x_0=1/(N+1)$ corresponding to $N=108, 256,$ and 500 where extrapolated to $x_2=0$. The results of these extrapolations are listed in Table VIII.

- ¹R. M. Stratt and M. Maroncelli, *J. Phys. Chem.* **100**, 12981 (1996).
²(a) J. P. Hansen and I. R. McDonald, *Theory of Simple Liquids* (Academic, New York, 1976); (b) C. G. Gray and K. E. Gubbins, *Theory of Molecular Fluids*, Fundamentals Vol. 1 (Clarendon, Oxford, 1984); (c) M. P. Allen and D. J. Tildesley, *Computer Simulation of Liquids* (Clarendon, Oxford, 1987).
³(a) G. Stell, J. C. Rasaiah, and H. Narang, *Mol. Phys.* **23**, 393 (1972); (b) B. Larsen, J. C. Rasaiah, and G. Stell, *ibid.* **33**, 987 (1977); (c) G. Stell, in *Statistical Mechanics. Part A: Equilibrium Techniques*, edited by B. J. Berne (Plenum, New York, 1977).
⁴(a) M. S. Wertheim, *Mol. Phys.* **37**, 83 (1979); (b) V. Venkatasubramanian, K. E. Gubbins, C. G. Gray, and C. G. Joslin, *ibid.* **52**, 1411 (1984); (c) C. G. Joslin, C. G. Gray, and K. E. Gubbins, *ibid.* **54**, 1117 (1985); (d) C. Kriebel and J. Winkelmann, *ibid.* **88**, 559 (1996).
⁵(a) D. V. Matyushov and R. Schmid, *J. Chem. Phys.* **105**, 4729 (1996); (b) D. V. Matyushov and B. M. Ladanyi, *ibid.* **107**, 1362 (1997); (c) **107**, 1375 (1997).
⁶(a) A. Papazyan and A. Warshel, *J. Chem. Phys.* **107**, 7975 (1997); (b) A. Papazyan and A. Warshel, *J. Phys. Chem. B* **101**, 11254 (1997).
⁷We do not consider here nonpolar solvation mechanisms chiefly caused by dispersion forces.
⁸(a) B. Jayaram, R. Fine, K. Sharp, and B. Honig, *J. Phys. Chem.* **93**, 4320 (1989); (b) B. Roux, H.-A. Yu, and M. Karplus, *ibid.* **94**, 4683 (1990); (c) S. W. Rick and B. J. Berne, *J. Am. Chem. Soc.* **116**, 3949 (1994); (d) J.-K. Hyun and T. Ichiye, *J. Chem. Phys.* **109**, 1074 (1998).
⁹(a) J. S. Bader and B. J. Berne, *J. Chem. Phys.* **104**, 1293 (1996); (b) J. S. Bader, C. M. Cortis, and B. J. Berne, *ibid.* **106**, 2372 (1997).
¹⁰(a) C. J. F. Böttcher, *Theory of Electric Polarization* (Elsevier, Amsterdam, 1973), Vol. 1; (b) L. D. Landau and E. M. Lifshitz, *Electrodynamics of Continuous Media* (Pergamon, Oxford, 1960).
¹¹(a) W. R. Fawcett and A. Kloss, *J. Phys. Chem.* **100**, 2019 (1996); (b) L. Luo, H. Ågren, and K. V. Mikkelsen, *Chem. Phys. Lett.* **275**, 145 (1997).
¹²(a) D. Levesque, G. N. Patey, and J. J. Weis, *Mol. Phys.* **34**, 1077 (1977); (b) G. N. Patey, D. Levesque, and J. J. Weis, *ibid.* **45**, 733 (1982); (c) S. W. de Leeuw, J. W. Perram, and E. R. Smith, *Proc. R. Soc. London, Ser. A* **388**, 177 (1983).
¹³(a) E. L. Pollock and B. J. Alder, *Physica A* **102**, 1 (1980); (b) M. Neumann, *Mol. Phys.* **50**, 841 (1983); (c) C. G. Gray, Y. S. Sainger, C. G. Joslin, P. T. Cummings, and S. Goldman, *J. Chem. Phys.* **85**, 1502 (1986).
¹⁴(a) P. G. Kusalik, *J. Chem. Phys.* **93**, 3520 (1990); (b) *Mol. Phys.* **80**, 225 (1993); (c) P. G. Kusalik, M. E. Mandy, and I. M. Svishchev, *J. Chem. Phys.* **100**, 7654 (1994).
¹⁵S. W. de Leeuw, J. W. Perram, and E. R. Smith, *Annu. Rev. Phys. Chem.* **37**, 245 (1986).
¹⁶G. Stell, G. N. Patey, and J. S. Høye, *Adv. Chem. Phys.* **18**, 183 (1981).
¹⁷(a) M. S. Skaf, T. Fonseca, and B. M. Ladanyi, *J. Chem. Phys.* **98**, 8929 (1993); (b) A. Luzar, A. K. Soper, and D. Chandler, *ibid.* **99**, 6836 (1993); (c) M. S. Skaf and B. M. Ladanyi, *ibid.* **102**, 6542 (1995); (d) B. M. Ladanyi and M. S. Skaf, *Annu. Rev. Phys. Chem.* **44**, 335 (1993); (e) M. S. Skaf, *Mol. Phys.* **90**, 25 (1990); (f) I. P. Omelyan, *ibid.* **93**, 123 (1998).
¹⁸G. N. Patey, D. Levesque, and J. J. Weis, *Mol. Phys.* **38**, 219 (1979).
¹⁹P. H. Fries and G. N. Patey, *J. Chem. Phys.* **82**, 429 (1985).
²⁰(a) A. Tani, D. Henderson, and J. A. Barker, *Mol. Phys.* **48**, 863 (1983); (b) S. Goldman, *ibid.* **71**, 491 (1990).
²¹M. Neumann, *Mol. Phys.* **57**, 97 (1986).

- ²²A. Gil-Villegas, S. C. McGrother, and G. Jackson, *Mol. Phys.* **92**, 723 (1997).
- ²³P. H. Fries, J. Richardi, and H. Krienke, *Mol. Phys.* **90**, 841 (1997).
- ²⁴D. Wei, G. N. Patey, and A. Perera, *Phys. Rev. E* **47**, 506 (1993).
- ²⁵Our effective radius differs from that introduced by Bader and Berne (Ref. 9) for dipolar solutes $R_{\text{eff}}^{-1} = \int_0^\infty (dr/r^2) g_{0s}(r)$. The latter definition follows from a perturbation expansion for the solvation chemical potential of a spherical ion and not of a dipole.
- ²⁶The previous publication [Ref. 5(a)] contains a sign misprint in the tabulation of the integral $I_{0s}^{(3)}$. The integral was approximated by a polynomial in $1/r_{0s}$, $I_{0s}^{(3)} = a(\rho^*)/r_{0s}^3 + b(\rho^*)/r_{0s}^4 + c(\rho^*)/r_{0s}^6$. In the polynomial fit $c(\rho^*) = c_0 + c_1\rho^* + c_2\rho^{*2} + c_3\rho^{*3}$ the coefficient c_3 should be +0.0983 instead of -0.0983 as in Ref. 5(a).
- ²⁷(a) L. Verlet and J.-J. Weis, *Phys. Rev. A* **5**, 939 (1972); (b) L. L. Lee and D. Levesque, *Mol. Phys.* **26**, 1351 (1973).
- ²⁸(a) T. Boublik, *J. Chem. Phys.* **53**, 471 (1970); (b) G. A. Mansoori, N. F. Carnahan, K. E. Starling, and T. W. Leland, *ibid.* **54**, 1523 (1971).
- ²⁹D. V. Matyushov and B. M. Ladanyi, *J. Chem. Phys.* **107**, 5815 (1997).
- ³⁰D. V. Matyushov and B. M. Ladanyi (unpublished).
- ³¹(a) D. Wei and G. N. Patey, *Phys. Rev. Lett.* **68**, 2043 (1992); (b) *Phys. Rev. A* **46**, 7783 (1992); (c) G. Ayton and G. N. Patey, *Phys. Rev. Lett.* **76**, 239 (1996).
- ³²We used the untruncated solute-solvent dipole-dipole potential in the RHNC calculations. For comparison with simulations, however, a truncated potential with RF boundary conditions should be used instead. The potential truncation produces only a negligible result for the box size employed in the simulations.
- ³³L. Onsager, *J. Chem. Soc.* **58**, 1486 (1936).
- ³⁴(a) P. G. Wolynes, *J. Chem. Phys.* **86**, 5133 (1987); (b) L. Blum and W. R. Fawcett, *J. Phys. Chem.* **96**, 408 (1992).
- ³⁵The correlation length Λ_p appears in the MSA theory when the exponential decay is assumed for the fluctuations of the longitudinal polarization $\delta P_L(\mathbf{r})$ of the homogeneous dipolar liquid: $\langle \delta P_L(\mathbf{r}) \delta P_L(0) \rangle = \exp[-r/\Lambda_p]$. The exponential decay appears when the k -expansion of the Fourier transform of the direct correlation function at small k is truncated after $\propto k^2$ term.
- ³⁶This conclusion concerns only the effective cavity radius in dipole solvation. For solvation of small ions in water Roux *et al.* [Ref. 8(b)] showed that one can get relatively accurate estimates for the free energy of solvation when using the position of the first maximum of the site-site PDF (RISM-HNC) as an effective ionic radius.
- ³⁷(a) F. Garisto, P. G. Kusalik, and G. N. Patey, *J. Chem. Phys.* **79**, 6294 (1983); (b) H.-A. Yu and M. Karplus, *ibid.* **89**, 2366 (1988); (c) N. M. Cann and G. N. Patey, *ibid.* **106**, 8165 (1997).
- ³⁸D. Isbister and R. J. Bearman, *Mol. Phys.* **28**, 1297 (1974).
- ³⁹(a) B. Guillot and Y. Guissani, *J. Chem. Phys.* **99**, 8075 (1993); (b) N. Matubayasi, L. H. Reed, and R. M. Levy, *J. Phys. Chem.* **98**, 10640 (1994); (c) E. Grunwald and C. Steel, *J. Am. Chem. Soc.* **117**, 5687 (1995).
- ⁴⁰In treating experimental data, one usually considers a relation between enthalpy and entropy. For solvation thermodynamics due to the attraction potential considered here there is a nonzero but usually a very small difference between the internal energy and enthalpy. This difference is, however, much more substantial for the repulsive part of the intermolecular potential [Ref. 5(a)].
- ⁴¹D. V. Matyushov, *Chem. Phys.* **174**, 199 (1993).
- ⁴²H.-X. Zhou and A. Szabo, *J. Chem. Phys.* **103**, 3481 (1995).
- ⁴³T. Fonseca, B. M. Ladanyi, and J. T. Hynes, *J. Phys. Chem.* **96**, 4085 (1992).
- ⁴⁴D. V. Matyushov, R. Schmid, and B. M. Ladanyi, *J. Phys. Chem.* **101**, 1035 (1997).